Reproductive Biology and Endocrinology

RESEARCH Open Access

A dual-drug strategy to enhance the function of cryopreserved ovaries by promoting revascularization and inhibiting follicle over-activation

Lingyu Li[1,2†], Jian Yang[1†], Longzhong Jia[1,3], Jing Liang[1], Kaixin Cheng[1], Xuebing Yang[1], Lu Mu[1], Ge Wang[1], Kaiying Geng[1], Qiuxian Hu[1], Xueqiang Xu[1,4,5], Zhen Li[1], Guoliang Xia[1], Ting Guo[2], Jiawei Zhang[6*], Yan Zhang[1*] and Hua Zhang[1*]

Abstract

Background Ovarian tissue cryopreservation and transplantation (OTCT) is a promising approach for fertility preservation. However, significant follicle loss after transplantation challenges long-term reproductive recovery. Although primordial follicle loss and ischemic damage are known contributors, the underlying mechanisms and effective strategies to mitigate these damages are still lacking.

Methods Ovarian tissues from wild-type or *Tek-CreER*^{T2}*;mTmG* female mice were cryopreserved using vitrification. Follicle dynamics after OTCT were analyzed through histology, proteomics, and high-resolution imaging. To assess protective effects, cryopreserved ovaries were treated with 500 nM rapamycin (Rapa), an inhibitor of primordial follicle activation; 5 ng/mL vascular endothelial growth factor A (VEGFA), which promotes angiogenesis; or both (Cryo + VRCS, VEGFA-Rapa Combination Strategy). DMSO or H_2O served as controls. Grafts were collected at 3, 7, 14, and 120 days post-transplantation, with measurements of vascular density, tip cell density, follicle activation, and remaining follicles. Oocyte quality was evaluated via in vitro fertilization, and graft lifespan was estimated through estrous cycle monitoring.

Results Our study observed a rapid decline in follicle numbers shortly after transplantation in a mouse model. Proteomic analysis and high-resolution 3D imaging revealed that this depletion was primarily due to damage to tip cells, which are crucial for angiogenesis, and the overactivation of dormant primordial follicles. Damage to tip cells compromised vascular reconstruction, leading to ischemic injury, while mechanical handling during tissue isolation

†Lingyu Li and Jian Yang contributed equally to this work.

*Correspondence:
Jiawei Zhang
cbsjiaweizhang@163.com
Yan Zhang
yanzhang1011@cau.edu.cn
Hua Zhang
huazhang@cau.edu.cn

Full list of author information is available at the end of the article

and cryopreservation triggered excessive follicle activation. We implemented a combination therapy using rapamycin to inhibit follicle activation and VEGFA to promote angiogenesis prior to transplantation. This approach significantly improved follicle survival, extended reproductive function, and enhanced oocyte quality.

Conclusion Our study provides a practical strategy for preserving the reproductive potential of cryopreserved ovarian tissues by simultaneously targeting vascular integrity and follicle stability through the dual drug strategy of VEGFA and rapamycin combine treatment.

Keywords Ovarian cryopreservation, 3D high resolution imaging, Tip cell, Long-term fertility preservation, Primordial follicle activation

Background

Ovarian follicles are essential functional units of female fertility but are highly vulnerable to chemotherapy-induced damage, often leading to infertility in cancer patients [1, 2]. Many of these patients wish to have biological children after treatment, highlighting the need for effective fertility preservation strategies [3]. While conventional methods like oocyte and embryo cryopreservation are widely used, ovarian tissue cryopreservation followed by auto-transplantation has emerged as a promising alternative [3]. This approach preserves both the ovarian follicles and the surrounding stromal cells, which are crucial for endocrine function and follicle support [4]. Clinical studies have shown that ovarian tissue cryopreservation and transplantation (OTCT) can restore endocrine function in almost 100% of cases [5], with reported live birth rates near 41% [6], demonstrating its potential to improve the quality of life for cancer survivors. However, as OTCT gains wider clinical application, its limitations have become evident, particularly the limited longevity of transplanted tissue. Studies indicate that OTCT extends the reproductive lifespan by only 2–5 years on average [7, 8], primarily due to rapid depletion of the ovarian reserve during the critical period immediately after transplantation [9]. Ischemic injury and inadequate vascularization are key factors contributing to this rapid loss of follicle viability [9, 10]. Although some methods have been explored to mitigate these effects [11–13], current strategies have not yet efficiently addressed both the overactivation of dormant primordial follicles and the damage to the vascular network.

Maintaining vascular integrity is vital for the long-term survival of transplanted ovarian tissue, as angiogenesis plays a crucial role in reestablishing blood flow to the graft [14, 15]. Follicle-secreted factors, such as vascular endothelial growth factor A (VEGFA) are essential for stimulating the formation of new blood vessels [16, 17]. The combined application of angiogenic factors, including basic fibroblast growth factor (bFGF) and VEGFA, significantly enhances the vascular density of vitrified-thawed human ovarian tissue following xenotransplantation [18]. Recent studies have also show that co-transplanting frozen ovarian tissue with adipose tissue-derived mesenchymal stem cells that secrete VEGFA promotes revascularization of the tissue [19]. These findings suggest that promoting angiogenesis can help alleviate ischemia and improve the supply of oxygen and nutrients to the graft, thereby enhancing follicle survival [20]. However, the optimal approach for integrating angiogenesis support with strategies to inhibit primordial follicle activation during OTCT has not been thoroughly explored.

In parallel with addressing vascular integrity, managing the activation of dormant primordial follicles is also crucial for preserving the ovarian reserve [21]. Under physiological conditions, the activation of primordial follicles is tightly regulated by the mTORC1-PI3K signaling pathway in pre-granulosa cells. In response to extracellular signals such as stress, nutrients, oxygen, and cytokines, the mTOR pathway in pre-granulosa cells is activated, leading to the production of KIT ligand. This activates the PI3K pathway in oocytes, resulting in the phosphorylation of FOXO3A, translocates to the cytoplasm, and a relief of its inhibitory effect on oocyte growth, thereby initiating primordial follicle activation [22]. Mechanical damage during ovarian tissue handling, exposure to cryoprotectant toxicity, and hypoxic stress post-transplantation can all trigger the overactivation of primordial follicles, which can rapidly deplete the ovarian reserve, as activated follicles enter an irreversible growth phase [23]. Inhibiting mTORC1 activity with drugs like rapamycin has shown promise in preventing premature primordial follicle activation. For instance, incubating mouse ovaries in a medium containing 750 nM rapamycin prior to cryopreservation [24], or adding 1 μM rapamycin to the transport and freezing solutions, significantly inhibits the activation of the mTOR signaling pathway, reducing excessive primordial follicle activation induced by cryopreservation [25]. However, since the activation process is transient and can be exacerbated by mechanical stress during tissue manipulation [26]. It is essential to apply inhibitory treatments early and consistently throughout the OTCT process.

In this study, we aimed to develop a strategy to improve the follicular survival rate of OTCT. Drawing on previous findings, we hypothesized that preventing premature

activation of primordial follicles and promoting early revascularization could help preserve follicle viability and improve graft outcomes. To test this, we employed a mouse model and performed proteomic analyses to monitor follicle loss and investigate the underlying mechanisms of follicular depletion post-OTCT. Based on our results, we proposed a dual-drug strategy combining rapamycin, to suppress primordial follicle overactivation, and VEGFA, to stimulate angiogenesis. This approach significantly reduced follicle loss, prolonged the functional lifespan of the graft, and improved oocyte quality, offering a promising solution for preserving ovarian reserve during OTCT.

Materials and methods

Animals

Young adult (6–8 weeks) and adolescent (PD21) female C57BL/6 N mice were purchased from Beijing Vital River Laboratory Animal Technology Co., Ltd. The *Tek-CreER^{T2}* mice were purchased from National Applied Research Laboratories, Taiwan, China, express a *Cre-ER^{T2}* recombinase under the control of *tek* promoter, which is known to be expressed in vascular endothelial cells. *mTmG* mice (strain 007576, Jackson Laboratory) were generated as previously described [27]. To obtain *Tek-CreER^{T2}*; *mTmG* mice, male *Tek-CreER^{T2}* mice were crossed with female *mTmG* mice, resulting in offspring with vascular endothelial cells labeled with green fluorescence following Tamoxifen (40 mg/kg.BW, 10540-29-1, Sigma-Aldrich) induction [28]. All mice were housed in Laboratory Animal Center, College of Biology, China Agricultural University, under specific pathogen-free (SPF) conditions. The facility maintained a strictly controlled environment with a 12-hour light-dark cycle, temperature set at 26 °C, and humidity between 40% and 70%. Mice had ad libitum access to food and water. All animal experiments were approved by the Committee on the Ethics of Animal Experiments at China Agricultural University, NO. AW11104202-3-1.

Collection of ovarian tissues

PD21 adolescent female C57BL/6 N mice were euthanized by cervical dislocation, and ovaries were excised from the abdominal cavity. Under a stereomicroscope (Stemi 305, Zeiss), ovarian bursa, adipose tissue, and connective tissue attached to the ovaries were dissected in sterile cold phosphate-buffered saline (PBS, pH 7.4), either with or without supplementation of dimethyl sulfoxide (DMSO, 196055, MP) or 500 nM rapamycin (AY-22989, Selleck), with dissecting needles.

Ovarian tissue cryopreservation and recovery

Cryopreservation and recovery methods were adapted from previous studies [24]. Briefly, intact ovaries were halved and equilibrated in two steps: 1, Equilibration in Vitrification Solution I (VS I), comprising Dulbecco's Modified Eagle Medium/Nutrient Mixture F-12 (DMEM/F12, 1320033, Invitrogen) supplemented with 20% fetal bovine serum (FBS, A5670701, Thermo Fisher), 7.5% DMSO, and 7.5% ethylene glycol (EG; 324558; Sigma-Aldrich) for 10 min. 2, Equilibration in Vitrification Solution II (VS II), containing DMEM/F12 supplemented with 20% FBS, 15% DMSO, 15% EG, and 0.25 M sucrose (S818046, Macklin) for 5 min. Following equilibration, the ovarian tissues were rapidly plunged into liquid nitrogen for two weeks. Ovarian tissues were recovered by sequentially transferring through thawing solutions with decreasing concentrations of sucrose (0.5 M, 0.25 M, 0.125 M and 0 M) in DMEM/F12 supplemented with 20% FBS, for 5 min per step. Finally, a sucrose-free medium was used to remove residual cryoprotective agents and sucrose. According to the experimental design, DMSO or rapamycin was optionally added to the vitrification and thawing solutions.

Ovarian tissue in vitro culture

Fresh or recovered ovarian tissues were cultured using a well-established in vitro organ culture system, as described in our earlier study [29]. Specifically, the ovarian tissues were placed on Millicell Cell Culture Inserts (PICM0RG50, Millipore) within 24-well cell culture plates (702001, NEST), and incubated with 400 µL of basal medium (DMEM/F12 supplemented with 10% FBS) at 37 °C, 5% CO_2, and saturated humidity for 6 h. Based on dose gradient experiments and reported study [30], the ovarian tissues were treated with or without 500 nM rapamycin (Cryo + Rapa), 5 ng/mL VEGFA (V4512, Sigma-Aldrich) (Cryo + VEGFA), or a combination of both (Cryo + VRCS, VEGFA-rapamycin Combination Strategy), with DMSO or H_2O as controls.

Ovarian tissue transplantation

The cultured ovarian tissues were transplanted into the renal capsule of young adult (6–8 weeks old) C57BL/6N female mice, following the protocol described in previous study [31]. In detail, the mice were anesthetized with Avertin (300 mg/kg; T48402, Sigma-Aldrich), and make a small incision in the capsule of the kidney, followed by placing the ovarian tissue under the renal capsule. Recipient mice were euthanized at 3, 7, 14 days post-transplantation and the grafts were then fixed in 4% paraformaldehyde (PFA, 30525-89-4, Santa Cruz) to assess follicle count and development.

Detection of estrus cycle

The estrus cycle stage of recipient mice was evaluated daily through morphological examination of vaginal epithelial cells, following established protocol [32].

Assessments were conducted between 15:00 and 17:00 each day, using the following procedure: step 1, collection of a vaginal smear with a medical cotton swab dipped in PBS, Step 2, hematoxylin staining of the collected sample, and step 3, microscopic examination of cell morphology to identify the estrous stage. The estrous cycle stages were classified into four phases based on cellular characteristics: Proestrus (P), characterized by presence of nucleated epithelial cells; Estrus (E), predominance of large, anucleated keratinized epithelial cells; Metestrus (M), identified by leukocytes; and Diestrus (D), characterized by the presence of neutrophils.

Histological staining and follicle counting

The harvested ovarian tissues were fixed in 4% PFA at 4 °C overnight, followed by dehydration and embedding in paraffin. The embedded tissues were then sectioned into 8 μm thick serial sections using a microtome and mounted onto glass slides. Hematoxylin staining was performed on these sections to facilitate visualization of the follicles. Follicle counts at various developmental stages were conducted based on granulosa cell morphology and the structure of layers surrounding the oocytes: primordial follicles were characterized by a single layer of squamous granulosa cells surrounding the oocyte, primary follicles contained either a combination of squamous and cuboidal granulosa cells or exclusively cuboidal granulosa cells around the oocyte, secondary follicles were defined by an oocyte surrounded by multiple layers of granulosa cells, while antral follicles were identified by the presence of pyknotic nuclei and a large cavity among granulosa cells. Primordial and primary follicles were quantified by counting their presence in every fifth section of each hemi-ovary and multiplying the count by five to estimate their total number. Secondary and antral follicles were counted in every section without extrapolation, only follicles containing visible oocytes with clearly visible nuclei indicated by Hematoxylin staining were counted, to avoid double counting. The total follicle count for each hemi-ovary was obtained by summing the follicle numbers across all developmental stages. The total follicle count for the entire ovary was calculated by combining the follicle counts of both hemi-ovaries from the same ovary. The follicle depletion rate refers to the ratio of the number of follicles consumed per day to the initial number of follicles at the time of transplantation (PD21 + 0 days).

Immunofluorescence and imaging

Ovarian tissue sections were first dewaxed in xylene and rehydrated through a gradient series of ethanol solutions. Antigen retrieval was conducted using a microwave treatment in citric acid buffer (pH 6.0). Sections were then blocked with 3% BSA for 1 h at room temperature to prevent nonspecific binding. Following blocking, sections were incubated overnight at 4 °C with primary antibodies: FOXO3A (dilution 1:300, 12829, Rabbit, Cell Signaling Technologies) and DDX4 (dilution 1:300, ab27591, mouse, Abcam). After three PBS washes, sections were incubated at room temperature for 1 h with Alexa Fluor 555-conjugated donkey anti-mouse or 488-conjugated donkey anti-rabbit secondary antibodies (dilution 1:100, Life Technologies). Nuclear staining was completed using Hoechst 33,342 (dilution 1:100, C1022, Beyotime). Histological imaging was conducted using an inverted Leica (DMi8) and Andor Dragonfly spinning-disc confocal microscope and image analysis was performed using ImageJ software to assess primordial follicle activation and other relevant parameters. Ovarian sections for immunofluorescence and follicle counting were obtained from different ovaries, but they underwent identical processing procedures.

Transparency and high-resolution 3D imaging of ovarian tissues and grafts

The tissue clearing protocol was modified from a previously described method [15]. In detail, 40% (v/v) N-methylacetamide stock solution (M26305, Sigma-Aldrich) was prepared by diluting melted N-methylacetamide in phosphate-buffered saline (PBS). Histodenz (D2158, Sigma-Aldrich) was dissolved into to a concentration of 86% (w/v) with N-methylacetamide stock solution. To generate the final clearing solution, Triton X-100 (0.1% v/v) and 1-thioglycerol (M1753, Sigma-Aldrich) (0.5% v/v) were added to the Histodenz solution.

For visualization of the ovarian vascular network, ovarian tissues or grafts were harvested and washed in PBS containing 0.2% Triton X-100 and 0.5% 1-thioglycerol. This washing step was performed for 24 h at room temperature in the dark to remove residual blood cells. Following this, the tissues were immersed in the clearing solution at 1:50 (v/v) and incubated for 48 h in the dark at room temperature while rotating. Cleared ovarian tissues were mounted in a 35-mm dish with a 14-mm glass bottom (D35-14-1-N, Cellvis) containing fresh clearing solution for imaging.

High-resolution 3D imaging was performed using an Andor Dragonfly spinning-disc confocal microscope equipped with a ×40 objective, a scientific complementary metal-oxide semiconductor (sCMOS) camera (Andor Zyla 4.2), and an Andor Integrated Laser Engine (ILE) system with excitation lines at 405 nm (Hoechst), 488 nm, and 568 nm (mT). A spinning-disc confocal scan head (Andor Dragonfly 500) was used to enhance image acquisition efficiency and quality. Images were captured using Fusion 2.1 software (https://andor.oxinst.com/products/dragonfly#fusion) [33].

Post-acquisition image processing was performed using ImageJ software (http://rsbweb.nih.gov/ij/). All z-stacks

were projected, and color channels were merged to generate comprehensive 3D representations of the vascular network. Vascular density was calculated as the ratio of the green fluorescent vascular area to the total ovarian tissue area (%). To improve visualization, only the green fluorescence channel was displayed. Additionally, to clearly highlight the filopodia structures of tip cells, the mG (488 nm) channel was inverted to black and white using ImageJ software.

Quantification of tip cell numbers

Quantitative analysis of tip cells was conducted using reconstructed 3D ovarian imaging data. The images were analyzed using Imaris software (https://imaris.oxinst.com/) under the 3D View and Slice modes. The whole-mount imaging data were divided into optical stacks of approximately 50 μm along the z-axis. GFP-labeled blood vessels were manually examined in randomly selected optical stacks, with filopodia identified using the filament-tracing function in Imaris. To quantify tip cell density, the number of tip cells was counted within randomly selected regions of ovarian tissues or grafts. Each analyzed region had a defined volume of 500 μm × 500 μm × 50 μm, with 5 to 10 regions assessed per ovary ($n \geq 3$ ovarian tissues for each group). The density of tip cells was calculated by dividing the total number of tip cells in the selected regions by the corresponding tissue volume.

In vitro fertilization

14 days after transplantation, recipient mice were intraperitoneally administered with 250 IU/kg pregnant mare serum gonadotropin (PMSG, Sansheng Biological Technology), followed 46–48 h later by an additional injection of human chorionic gonadotropin (hCG, Sansheng Biological Technology). Cumulus-oocyte complexs (COCs) were retrieved under renal capsule 13 h post-hCG injection, and the number of MII oocytes was recorded. MII oocytes were collected and placed in HTF medium (M1130, Aibei Biological Technology). Sperm isolated from the epididymis of male mice were incubated in HTF medium for 30 min to complete capacitation. For in vitro fertilization, capacitated sperm were combined with MII oocytes in HTF fertilization medium. Four hours later, zygotes were transferred into a KSOM medium (M1430, Aibei Biological Technology) droplet covered with mineral oil (M8410, Sigma-Aldrich) for further culture. Approximately 16 h after fertilization, the number of two-cell embryos was recorded. Embryos were then cultured further, and the number of blastocysts was determined as described in previous studies [34].

Extraction and purification of total proteins

Protein sample preparation protocol was adapted from previously published methods [35]. The fresh or cryopreserved ovarian tissues were homogenized in RIPA lysis and extraction buffer (89900, Thermo Fisher) in 1.5 mL centrifuge tubes on ice. The samples were further disrupted using a pre-cooled ultrasonic disruptor for 40 min at 70% power, with 20-second pulses followed by 40-second intervals. Following sonication, the samples were centrifuged at 14,000 rpm for 10 min, and the resulting supernatant was collected as the total protein extract. Protein concentrations were measured by BCA assay KIT (5000201, Bio-Rad), and standardized to equal levels. Equal volumes of all samples were then washed by 8 M urea for three times to remove the remaining detergent (especially SDS) digested by trypsin (protein: enzyme = 50:1) overnight at 37 ℃. The proteins were then loaded onto a Q exactive mass spectrometer to obtain protein expression profiles.

Protein mass spectrometry

LC–MS analysis was conducted using a Waters nanoAcquity nanoHPLC (Waters, Milford, MA, USA) coupled with a Q-Exactive high-resolution mass spectrometer (Thermo Scientific, Waltham, MA, USA). Peptides were loaded onto a trap column (Acclaim PepMap100, 75 μm × 2 mm, Thermo Scientific, Waltham, MA, USA) and subsequently eluted onto a fused silica capillary packed with a 20 cm C18 stationary phase (Aqua C18, 3 μm, 125 Å, Phenomenex, Los Angeles, CA, USA). Elution was carried out using a 125-minute gradient. Mobile phases A and B consisted of 0.1% formic acid in water and acetonitrile, respectively, with a flow rate of 400 nL/min. The nanoESI voltage was set at 2.0 kV. Full mass scans were performed over the m/z range of 300–1800 with a resolution of 70,000 at m/z 200. MS/MS scans were obtained with a resolution of 17,500, targeting the top 10 most intense peptide signals, and a dynamic exclusion time of 20 s was applied.

Bioinformatics analysis

To assess the significance of the differences in protein expression, we used Student's t-test with a significance threshold set at $P < 0.05$ with Prism 9 for macOS (Version 9.2.0), and all results are presented as mean ± standard deviation (SD). Differentially expressed proteins (DEPs) were identified with a fold change > 1.5 and a P-value < 0.05, and visualized in a cluster heatmap. Further analysis of DEPs was conducted using Kyoto Encyclopedia of Genes and Genomes (KEGG) pathway enrichment and Gene Ontology (GO) enrichment through the Metascape platform [36]. Volcano plot, cluster heatmap, KEGG and GO enrichment visualizations were generated using tools available on the Bioinformatics website (https://www.bioinformatics.com.cn).

Experimental design and statistical rationale

The experimental design was aimed at evaluating protein expression differences between fresh and cryopreserved PD 21 mice ovarian tissues, using Label-free based mass spectrometry techniques. A minimum of 2 biological replicates ($n = 2$ ovaries for each sample) were included in each group. The rationale for this sample size was based on statistical power analysis. We employed fresh ovarian tissue as control group, to assess baseline protein expression levels and to account for any experimental variability. Biological replicates were defined as independent samples obtained from different biological sources. The rationale for including both biological and technical replicates was to ensure robustness of the findings and assess both inter- and intra-sample variability. Protein identification and quantification were performed using PEAKS search engine (PEAKS studio 11, Bioinformatics Solutions Inc, Canada) for peak alignment, peak picking, and protein quantitation. The search parameters were set as (1) Specific enzyme: Trypsin, allowing a maximum of three missed cleavages. (2) Fixed modification: Carbamidomethylation at cysteine residues (C). (3) Variable modifications: Oxidation of methionine (M). (4) Parent MS mass tolerance: 10 ppm. (5) Fragment MS/MS mass tolerance: 0.02 Da. The data were matched against the Uniprot human database (45,182 sequences, 2018-06, https://www.uniprot.org/). Data points were excluded if the mass spectrometry signal was below the threshold or if any sample preparation anomalies were detected. All exclusions were applied consistently across the datasets. The use of Student's t-test was justified by the data following a normal distribution. A non-parametric approach was considered for data that did not meet normality assumptions. Peptide identifications were filtered using a 1% False Discovery Rate (FDR), with a decoy database employed to assess the FDR. Peptides with a confidence score greater than 31 were selected for further bioinformatics analysis. The mass spectrometric raw data were submitted in ProteomeXchange, and the PXD number is PXD061025 (https://www.iprox.cn/page/project.html?id=IPX0011049000).

Statistical and analysis

All experiments were conducted with at least three biological samples. Data were analyzed using GraphPad Prism (Version 9.2.0) and are presented as means ± standard deviation (SD). Statistical comparisons between two groups were performed using a Student's t-test, with significance set at $P < 0.05$. Statistical significance levels are denoted as follows: $^{*}P < 0.05$, $^{**}P < 0.01$, $^{***}P < 0.001$, and ns (not significant, $P \geq 0.05$).

Results

Rapid follicle loss in cryopreserved ovarian tissue due to impaired angiogenesis and abnormal primordial follicle activation

To investigate the mechanisms underlying follicle loss during OTCT, we established a mouse model using ovaries from adolescent female mice (Fig. 1A). The ovaries, which contained a high density of primordial follicles [37], were bisected to simulate clinical damage, cryopreserved, thawed, and then transplanted under the kidney capsule (Fig. 1A). Following transplantation, the cryopreserved ovarian tissue developed antral follicles (Fig. 1B, red arrows) and released mature (MII-stage) oocytes within 14 days post transplantation (Fig. 1C, left). These oocytes were successfully fertilized in vitro and progressed to blastocyst stage (Fig. 1C, middle and right), demonstrating that the cryopreservation and transplantation protocol effectively mimicked the clinical OTCT process.

To quantify the extent of follicle depletion, ovarian grafts were collected at 3, 7, and 14 days post-transplantation. DEAD-box Helicase 4 (DDX4) staining confirmed the presence of oocytes and follicles at all time points (Fig. 1D). Quantitative analysis revealed a rapid and substantial reduction in follicle numbers within the first three days in both cryopreserved and fresh ovaries (Fig. 1E, 0 days: 2756 ± 128 vs. 2790 ± 117; 3 days: 713 ± 94 vs. 1429 ± 113). The fresh ovarian grafts exhibited a loss of approximately half of follicles, whereas the cryopreserved ones experienced a more pronounced depletion, losing over two-thirds of their follicles (Fig. 1E). Notably, the rate of follicle loss was significantly higher in cryopreserved ovaries compared to fresh ones (Fig. 1F, 24.71 ± 1.13% vs. 17.58 ± 1.35% per day, 681 ± 31 vs. 490 ± 38 follicles per day) during 0–3 days. After this initial sharp decline, follicle loss continued at a slower, more gradual rate in both fresh and cryopreserved grafts (Fig. 1F, 3–7 days: 2.10 ± 0.98% vs. 1.21 ± 0.52% per day (33 ± 14 vs. 59 ± 27 follicles per day); 7–14 days: 1.70 ± 0.53% vs. 1.37 ± 0.53% per day (38 ± 15 vs. 49 ± 16 follicles per day)). These results indicate that the most critical period for follicle loss occurs early post-transplantation, and that cryopreservation exacerbates the depletion.

To elucidate the mechanisms driving this rapid loss, we conducted a proteomic analysis using mass spectrometry (Figure S1A). A total of 610 differentially expressed proteins (DEPs) were identified between cryopreserved and fresh ovarian tissues, with 242 upregulated and 368 downregulated in the cryopreserved samples (Fig. 1G, Table S1). Cluster analysis revealed distinct protein expression profiles between the two groups (Fig. 1H). KEGG enrichment analysis demonstrated that the DEPs were significantly associated with pathways related to

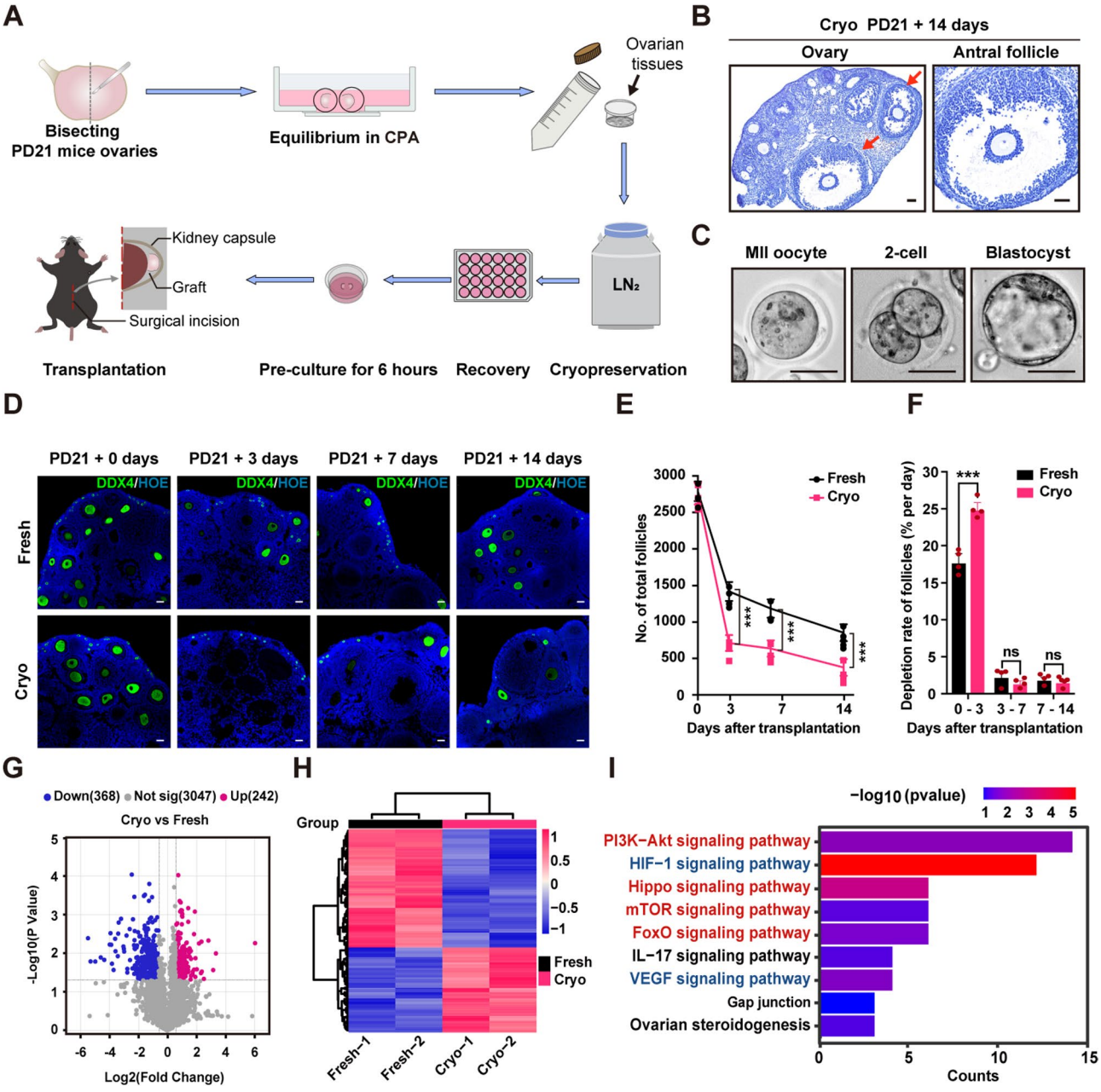

Fig. 1 Rapid follicle loss in cryopreserved ovarian tissues within three days post-transplantation. **A**, Overview of the cryopreservation and transplantation process: adolescent (PD21) ovaries were cryopreserved, thawed, pre-cultured, and transplanted under the kidney capsule. **B**, Hematoxylin staining showed antral follicles (red arrows) in cryopreserved ovaries 14 days after transplantation (PD21 + 14 days). **C**, MII oocytes (left) derived from cryopreserved tissues developed into two-cell embryo (middle) and blastocyst (right) following superovulation and in vitro fertilization. **D**, DDX4 immunostaining (green) revealed fewer follicles in cryopreserved ovaries compared to fresh controls at 3, 7 and 14 days post-transplantation. Nuclei were counterstained with Hoechst (HOE, blue). **E**, Follicle numbers dropped in both cryopreserved and the fresh ovarian grafts at 3, 7, and 14 days after transplantation, with the most rapid decline occurring within the first three days ($n \geq 4$ per group per time point). **F**, Follicle depletion rate was significantly higher in cryopreserved ovaries than in fresh controls during the first three days ($n = 3$ per group per time point). **G**, Volcano plot showing 368 downregulated and 242 upregulated proteins in cryopreserved ovaries compared to fresh ovaries. **H**, Heat map illustrating the different protein expression profiles between the two groups. **I**, KEGG enrichment analysis of differentially expressed proteins (fold change > 1.5, $n = 2$ for each group, $P < 0.05$), highlighting pathways related to angiogenesis (blue texts), and primordial follicle activation (red texts). Data are presented as mean ± SD from three independent biological replicates in (**E**) and (**F**). Statistical significance was determined using a two-tailed unpaired Student's t-test. ns, $P > 0.05$; ***$P < 0.001$. Scale bars: 50 μm

angiogenesis, including the "HIF-1 signaling pathway" and the "VEGF signaling pathway" (Fig. 1I, blue texts). Furthermore, Gene Ontology (GO) enrichment analysis highlighted terms related to vascular network development, such as "endothelial cell development," "negative regulation of angiogenesis," "negative regulation of blood vessel morphogenesis," and "blood vessel diameter maintenance" (Figure S1B, blue texts), suggesting that impaired angiogenesis may contribute to the rapid follicle loss.

In addition to angiogenesis-related changes, KEGG pathway analysis also revealed significant alterations in signaling pathways involved in the activation of primordial follicles, such as the "PI3K-Akt signaling pathway" and the "FoxO signaling pathway," which regulate the activation of dormant oocytes (Fig. 1I, red texts). Other pathways, including the "Hippo signaling pathway" and "mTOR signaling pathway" were also affected (Fig. 1I, red texts), reflecting changes in the activation state of pre-granulosa cells and their communication with surrounding tissues. These findings suggest that the accelerated follicle loss in cryopreserved ovarian tissue is likely driven by a combination of impaired vascular regeneration and abnormal activation of primordial follicles.

Cryopreservation-induced tip cell damage and primordial follicle over-activation contribute to rapid follicle loss during OTCT

To understand the mechanisms leading to impaired ovarian angiogenesis in cryopreserved ovarian tissues, we employed a *Tek-CreER^{T2};mTmG* endogenous fluorescent reporter mouse model. This model allows for high-resolution visualization of the vascular network by labeling all blood vessels in the ovarian tissue with membrane-localized GFP [15]. Using whole-mount imaging of transparent *Tek-CreER^{T2};mTmG* ovaries, we achieved subcellular resolution to identify key angiogenic cells, such as the leading tip cells [15] in both cryopreserved and fresh ovarian tissues (Fig. 2A). Our analysis showed a modest reduction in overall blood vessel density in cryopreserved ovaries compared to fresh controls (Fig. 2B and C, 61.66 ± 4.34% vs. 74.57 ± 3.22%), indicating structural damage to the vascular network caused by cryopreservation.

High-resolution imaging revealed a striking reduction in the number of tip cells with typical filopodia (Fig. 2D, red arrows) per unit volume in cryopreserved ovaries compared to fresh tissues (Fig. 2E, 1286.62 ± 267.59 vs. 5376.16 ± 1941.72 per mm^3). Notably, tip cells exhibited a 76.08% reduction (calculated from Fig. 2E), compared to only a 17.31% reduction in the existing ovarian vasculature (calculated from Fig. 2C) of cryopreserved ovarian tissues relative to fresh ones. This significant loss suggests that tip cells, which are crucial for initiating and guiding angiogenesis, are more susceptible to cryopreservation-induced damage than established endothelial cells. The increased vulnerability of tip cells likely contributes to the observed impairment in vascular remodeling post-transplantation, making tip cell damage a critical factor limiting angiogenesis in cryopreserved ovarian grafts.

To further investigate how this vascular impairment affects the regenerative capacity of the vascular network in transplanted cryopreserved ovaries, we conducted high-resolution whole-mount imaging three days after transplantation. Although the density of tip cells with typical filopodia (Fig. 2F, red arrows) increased in cryopreserved ovarian tissues three days post-xenotransplantation, their numbers remained significantly lower than in transplanted fresh ovaries (Fig. 2G, 5028.03 ± 997.49 vs. 7792.87 ± 2061.45 per mm^3). Similarly, the density of reconstructed blood vessels in cryopreserved ovarian grafts was substantially lower than in fresh ones (Fig. 2H and I, 32.97 ± 13.85% vs. 58.35 ± 10.97%). These findings indicate that cryopreservation-induced tip cell damage reduces the ovarian tissue's ability to reconstruct the vascular network and may therefore be a key factor contributing to the rapid depletion of the ovarian reserve following transplantation.

In addition to vascular damage, we examined the impact of cryopreservation on follicle dynamics, particularly the overactivation of primordial follicles, which accelerates follicle loss. Proteomic analysis suggested an increase in primordial follicle activation (Fig. 1I, red texts), prompting us to assess the expression and localization of Forkhead Box O3 (FOXO3A)—a key marker of primordial follicle activation [22]. FOXO3A typically resides in the nucleus of dormant oocytes but relocates to the cytoplasm upon activation [38, 39]. We compared the activation status of primordial follicles in in vivo ovaries, freshly isolated ovarian tissues subjected to mechanical handling, and cryopreserved ovarian tissues. A significantly higher proportion of cytoplasmic FOXO3A was observed in the primordial follicles of both freshly isolated and cryopreserved ovaries compared to in vivo ovaries at PD21 (Fig. 2J, white arrowheads; Fig. 2K, 22.53 ± 1.19% in freshly isolated group and 49.18 ± 1.93% in cryopreserved group vs. 4.98 ± 1.66% in in vivo control group). This finding indicates that both cryopreservation and mechanical manipulation during tissue preparation contribute to the overactivation of primordial follicles.

These results collectively highlight the dual detrimental effects of cryopreservation and mechanical stress on ovarian tissue integrity. Cryopreservation-induced damage to tip cells compromises angiogenesis and vascular remodeling, while both cryopreservation and tissue handling promote the overactivation of primordial follicles, accelerating follicle depletion. To protect the ovarian reserve during OTCT, strategies should prioritize

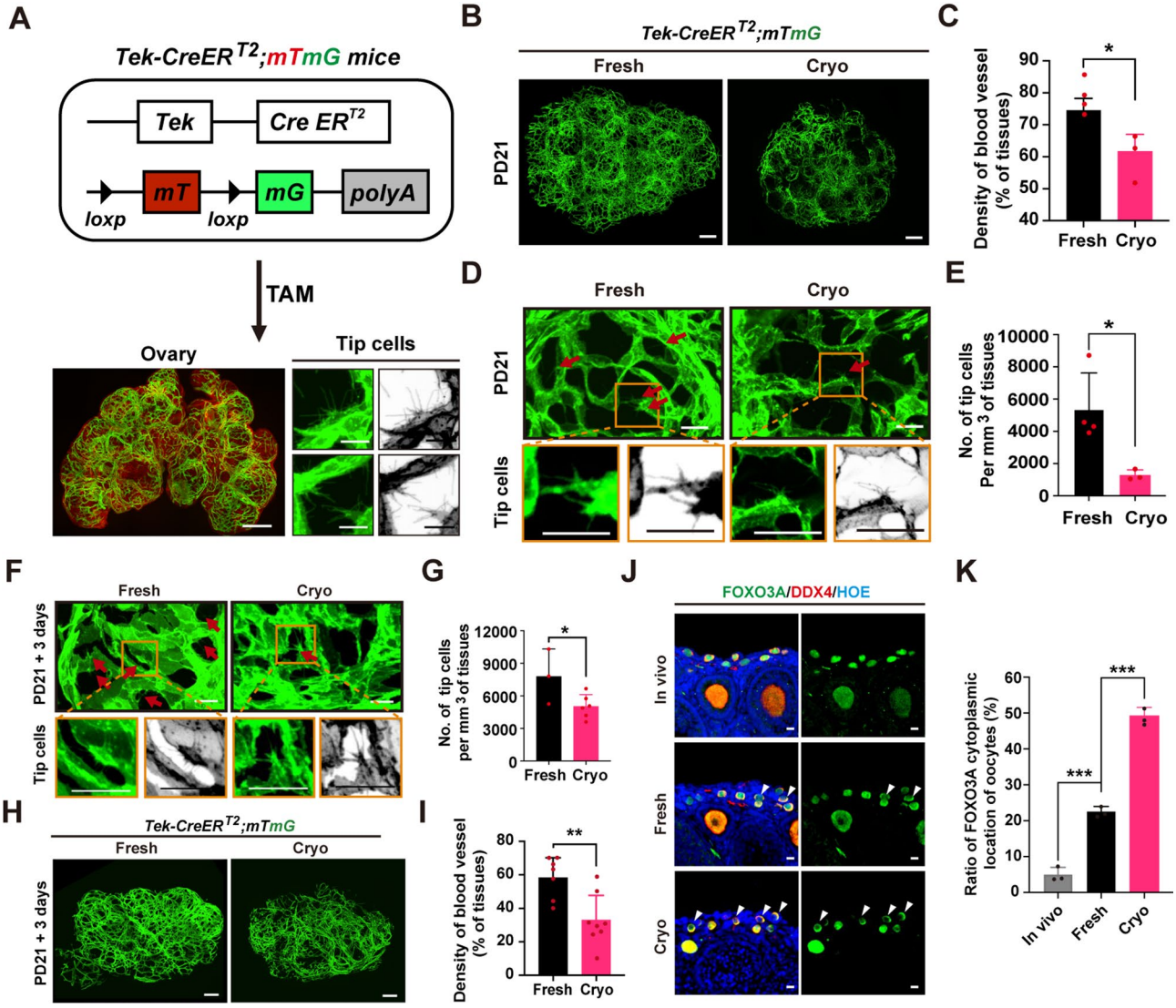

Fig. 2 Impaired angiogenesis and follicle overactivation in cryopreserved ovaries. **A**, Imaging strategy: *Tek-CreER*^{T2}*;mTmG* ovaries were labeled with mGFP to visualize blood vessels. 3D images were obtained using confocal microscopy. **B**, Vascular networks in fresh and cryopreserved ovaries after 6 h of culture. **C**, Vascular density was lower in cryopreserved ovaries compared to fresh (Fresh, $n=4$; Cryo, $n=3$). **D**, Tip cells (red arrows) in fresh and cryopreserved ovaries after 6 h of culture. **E**, Fewer tip cells were observed in cryopreserved ovaries than in fresh ovaries (Fresh, $n=4$; Cryo, $n=3$). **F**, Tip cells (red arrows) in grafts from fresh and cryopreserved ovaries, 3 days post-transplantation. **G**, Tip cell counts were lower in cryopreserved grafts compared to fresh grafts (Fresh, $n=3$; Cryo, $n=6$). **H**, Vascular networks in grafts from fresh and cryopreserved ovaries, 3 days post-transplantation. **I**, Blood vessel density was reduced in grafts from cryopreserved ovaries versus fresh (Fresh, $n=6$; Cryo, $n=8$). **J**, FOXO3A (Green) and DDX4 (red) immunostaining of in vivo, freshly isolated and cryopreserved ovaries showed cytoplasmic localization of FOXO3A (white arrowheads), indicating oocyte activation. **K**, The percentage of oocytes with cytoplasmic FOXO3A was higher in both freshly isolated and cryopreserved ovarian tissues compared to in vivo controls at PD21 ($n=3$ for each group). Data in (**C**), (**E**), (**G**), (**I**), and (**K**) are presented as mean ± SD. Statistical analysis was performed using a two-tailed unpaired Student's t-test; $^{*}P<0.05$, $^{**}P<0.01$, $^{***}P<0.001$. Scale bars: 100 µm in (**A**, bottom left), (**B**), (**H**), (**J**); 20 µm in (**A**, bottom right), (**D**), (**F**)

minimizing primordial follicle activation from the initial stages of tissue handling and isolation, alongside supporting angiogenesis.

Mitigating vascular damage and primordial follicle overactivation using VEGFA and rapamycin

Our study identified that rapid follicle loss in cryopreserved ovaries is driven by both vascular damage and overactivation of primordial follicles. To address vascular impairment, we treated recovered *Tek-CreER*^{T2}*;mTmG* ovaries with VEGFA (5 ng/mL), a known angiogenesis stimulator, for 6 h. High-resolution whole-mount imaging revealed a significant increase in vascular density in VEGFA-treated ovaries compared to controls (Fig. 3A and B, 78.25 ± 6.12% vs. 51.02 ± 3.97%), indicating that VEGFA can effectively improve vascular integrity. Additionally, VEGFA treatment resulted in a moderate increase the density of tip cells compared to

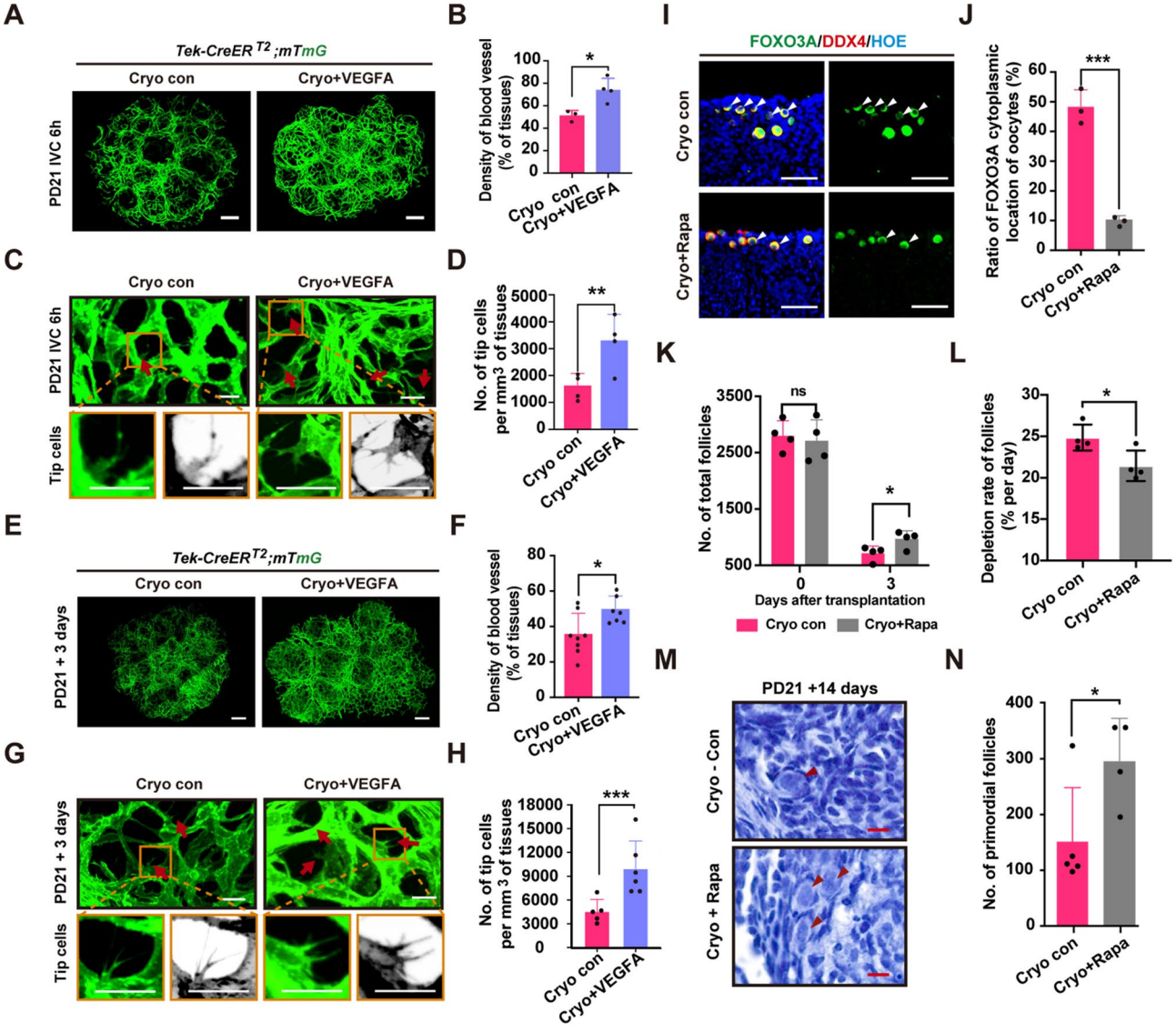

Fig. 3 VEGFA reduces vascular damage and rapamycin prevents follicle overactivation in cryopreserved ovaries. **A**, Vascular networks in cryopreserved PD21 *Tek-CreER*^{T2}*;mTmG* mouse ovaries with or without VEGFA treatment for 6 h. **B**, Blood vessel density was higher in VEGFA treated ovaries compared to controls (Cryo + H_2O, $n = 3$; Cryo + VEGFA, $n = 4$). **C**, Tip cells (red arrows) in cryopreserved PD21 *Tek-CreER*^{T2}*;mTmG* mouse ovaries with or without VEGFA treatment for 6 h. **D**, More tip cells were found in VEGFA pre-cultured ovaries than in controls ($n = 4$ for each group). **E**, Vascular networks in cryopreserved ovarian grafts treated with or without VEGFA at 3 days post-transplantation. **F**, Blood vessel density increased in VEGFA-treated grafts versus controls (Cryo + H_2O, $n = 8$; Cryo + VEGFA, $n = 7$). **G**, Tip cells (red arrows) in cryopreserved ovarian grafts treated with or without VEGFA at 3 days post-transplantation. **H**, Tip cell counts were higher in VEGFA-treated grafts compared to controls (Cryo + H_2O, $n = 5$; Cryo + VEGFA, $n = 6$). **I**, Immunostaining for FOXO3a (green) and DDX4 (red) less cytoplasmic translocation (white arrowheads) in rapamycin-treated ovaries, indicating reduced oocyte activation. **J**, The percentage of oocytes with cytoplasmic FOXO3a was lower in rapamycin-treated ovaries compared to controls ($n = 3$ for each group). **K**, More follicles were found in rapamycin-treated grafts than in controls at 3 days post-transplantation ($n = 4$ for each group). **L**, Follicle depletion rate was lower in rapamycin-treated grafts compared to controls ($n = 4$ for each group). **M**, Histology showed more primordial follicles (red arrowheads) in rapamycin-treated grafts at 14 days post-transplantation. **N**, More primordial follicles were present in rapamycin-treated grafts versus controls ($n = 4$ for each group). Data in (**B**), (**D**), (**F**), (**H**), (**J**), (**K**), (**L**) and (**N**) are presented as mean ± SD. Statistical analysis was performed using a two-tailed unpaired Student's t-test; ns, $P > 0.05$; *$P < 0.05$; **$P < 0.01$; ***$P < 0.001$. Scale bars: 100 μm in (**A**), (**E**), (**I**); 20 μm in (**C**), (**G**), (**M**)

controls (Fig. 3C, red arrows; Fig. 3D, 3274.55 ± 864.32 vs. 1594.13 ± 417.97 per mm^3), suggesting that short-term VEGFA exposure promotes angiogenesis by enhancing the recruitment of these key angiogenic cells.

To evaluate the long-term effects of VEGFA treatment on vascular development, we assessed the vascular network in transplanted cryopreserved ovaries three days post-transplantation. VEGFA-pretreated ovaries showed a significant enhancement in blood vessel density

compared to controls (Fig. 3E and F, 49.50 ± 7.13% vs. 32.97 ± 13.85%). The number of tip cells per cubic millimeter was also notably higher in VEGFA-treated grafts (Fig. 3G, red arrows; Fig. 3H, 8994.02 ± 4895.86 vs. 4996.05 ± 2640.24 per mm^3), demonstrating that VEGFA pre-treatment effectively mitigates cryopreservation-induced vascular damage and supports vascular network reconstruction.

To counteract the overactivation of primordial follicles, we used rapamycin, an mTORC1 inhibitor, throughout the ovarian tissue treatment process [40], including dissection, cryopreservation, recovery, and pre-culture. rapamycin treatment significantly reduced the ratio of cytoplasmic FOXO3A in oocytes, indicating a decrease in primordial follicle activation compared to control group (Fig. 3I, white arrowheads; Fig. 3J, 10.12 ± 1.26% vs. 48.19 ± 4.78%). Three days after transplantation, rapamycin-treated cryopreserved ovaries displayed a significantly higher number of surviving follicles compared to untreated controls (Fig. 3K, 965.50 ± 129.58 vs. 711.5 ± 114.10). The rate of follicle depletion was also slower in rapamycin-treated ovaries (Fig. 3L, 21.44 ± 1.60% vs. 24.86 ± 1.36% per day), indicating that rapamycin effectively protects against premature primordial follicle activation.

Further monitoring of follicle survival showed that more primordial follicles persisted in rapamycin-treated grafts even 14 days post-transplantation (Fig. 3M, red arrowheads; Fig. 3N, 298.5 ± 67.09 vs. 154 ± 86.47). These findings demonstrate that rapamycin effectively inhibits the overactivation of primordial follicles, thereby improving follicle survival and maintaining the ovarian reserve. Together, the results suggest that combining VEGFA to enhance angiogenesis and rapamycin to prevent primordial follicle activation is a promising strategy to mitigate the adverse effects of cryopreservation on ovarian tissue.

Enhancing ovarian reserve protection efficiency with the VEGFA-rapamycin combination strategy

Given the complementary protective effects of VEGFA and rapamycin on the ovarian reserve, we developed a dual-drug treatment approach, termed the VEGFA-Rapamycin Combination Strategy (VRCS), to improve follicle survival in cryopreserved ovarian tissues. In this approach, rapamycin was administered throughout the entire process, from tissue collection to cryopreservation, recovery, and pre-culture (Fig. 4A, red arrow), while VEGFA was added after tissue recovery and just before transplantation to further enhance follicle survival (Fig. 4A, green arrow).

To assess the effectiveness of VRCS, we compared follicle survival and development in cryopreserved ovaries post-transplantation, using rapamycin-only (Cryo + Rapa) treatment as a control. Three days post-transplantation, the VRCS group exhibited a higher number of follicles compared to the control group (Fig. 4B, 1197 ± 124.11 vs. 916 ± 104.45), resulting in a significantly lower follicle depletion rate (Fig. 4C, 18.84 ± 0.91% vs. 21.03 ± 0.85% per day). This protective effect persisted through 14 days post-transplantation, with a greater number of surviving primordial follicles in the VRCS group compared to the rapamycin-only group (Fig. 4D, red arrowheads; Fig. 4E, 329.4 ± 36.12 vs. 263.5 ± 40.56). These results indicate that VRCS provides more effective short-term protection for the ovarian reserve in cryopreserved ovarian tissues.

To evaluate the impact of VRCS on oocyte production and developmental potential, we performed superovulation on recipient mice 14 days after transplantation and harvested the oocytes from ovarian grafts (Fig. 4F, left). The VRCS group produced significantly more oocytes per ovary compared to the rapamycin-only group (Fig. 4G, 3.63 ± 0.96 vs. 1.5 ± 0.5 per ovary). Additionally, these oocytes demonstrated enhanced developmental potential, with a higher percentage developing into two-cell embryos (Fig. 4F, middle, red arrows; Fig. 4H, VRCS: 72.93 ± 8.17% vs. Rapa-only: 25.50 ± 10.52%) and blastocysts (Fig. 4F, right, blue arrows; Fig. 4H, VRCS: 46.25 ± 4.15% vs. Rapa-only: 12.5 ± 9.01%). These findings confirm that VRCS is superior to rapamycin-alone treatment in preserving both follicle survival and oocyte developmental competence.

Overall, the results demonstrate that the VRCS offers a more effective approach for maintaining the ovarian reserve and enhancing the quality of oocytes in cryopreserved ovarian tissues, providing a promising strategy for fertility preservation in clinical settings.

VRCS prolongs the maintenance of female reproductive function after OTCT

Building on the short-term benefits observed with the VRCS for cryopreserved ovarian tissue, we evaluated its long-term effects on ovarian reserve preservation. We transplanted cryopreserved ovarian tissues treated with different protocols (untreated, rapamycin alone, or VRCS) into the renal capsules of recipient mice and monitored their estrous cycles over a four-month period (Fig. 5A). In the untreated group, mice maintained regular estrous cycles (4–6 days per cycle) for up to 11 weeks, with the longest lasting 13 weeks (Fig. 5B). In contrast, the rapamycin-only treated group exhibited regular cycles for up to 16 weeks. Remarkably, mice treated with VRCS maintained consistent estrous cycles throughout the entire four-month observation period, indicating that VRCS significantly extends the functional lifespan of transplanted ovaries compared to rapamycin alone.

To assess the long-term preservation of the ovarian reserve, we collected the ovarian grafts after four months and performed histological analysis to evaluate

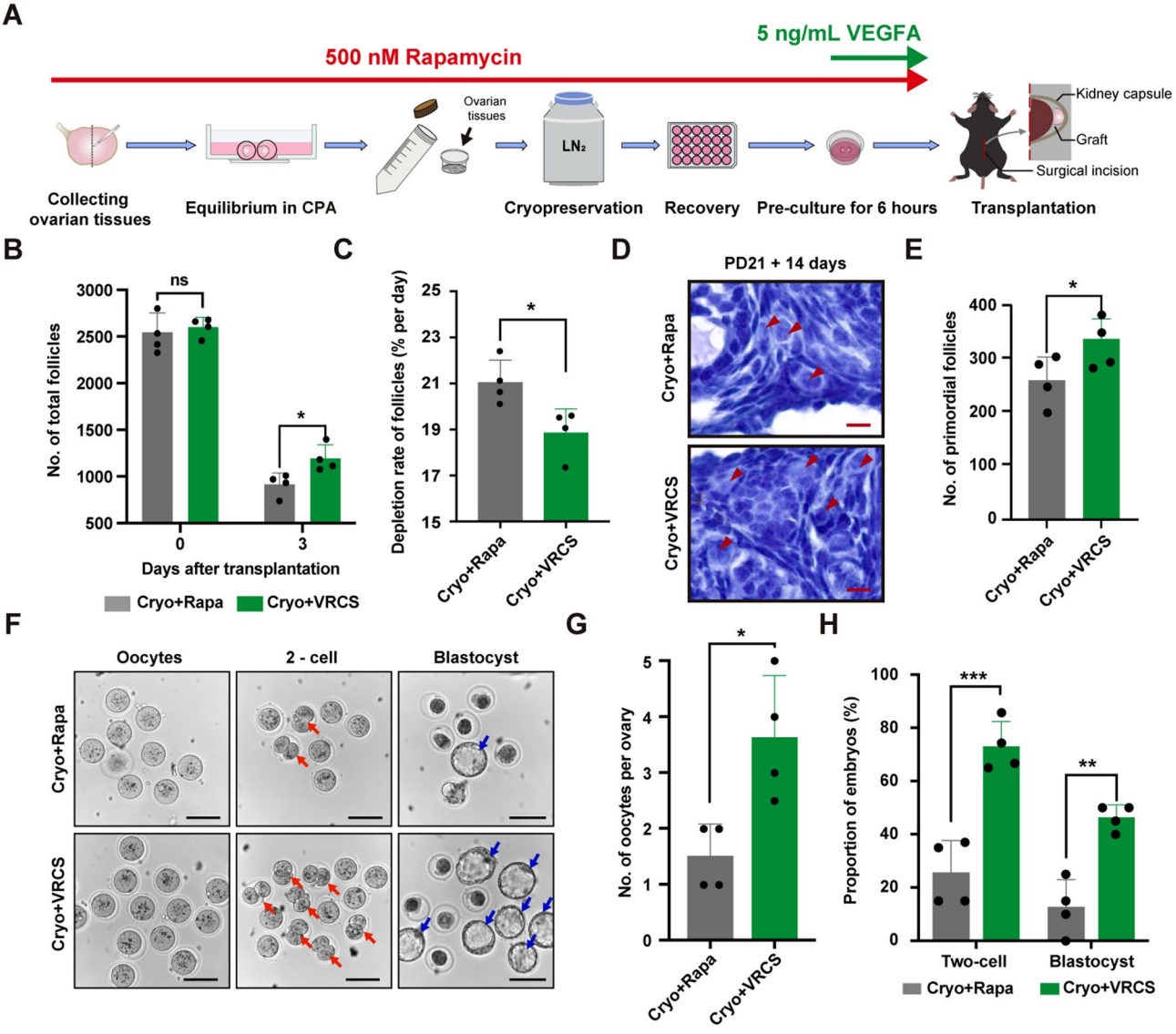

Fig. 4 VEGFA-Rapamycin combination strategy (VRCS) enhances ovarian reserve protection. **A**, Overview of the VRCS: 500 nM rapamycin was added throughout the process (red arrow) and 5 ng/mL VEGFA during pre-culture (green arrow). **B**, Follicle counts showed higher numbers in VRCS-treated grafts compared to rapamycin alone at 3 days post-transplantation ($n=4$ for each group). **C**, Follicle depletion rate (percent of follicle loss per day) was lower in VRCS-treated grafts than in rapamycin-only grafts at 3 days post-transplantation ($n=4$ for each group). **D**, Histology showing more primordial follicles (red arrowheads) in VRCS-treated grafts at 14 days post-transplantation. **E**, More primordial follicles were present in VRCS-treated grafts compared to rapamycin alone ($n=4$ for each group). **F**, Oocytes collected at 14 days post-transplantation (left) and two-cell embryos (middle, red arrows) and blastocysts (right, blue arrows) following in vitro fertilization. **G**, Oocyte quantification showed higher ovulation rates in VRCS-treated ovaries compared to rapamycin alone ($n=4$ for each group). **H**, Higher percentages of oocytes developed into two-cell embryos and blastocysts in VRCS-treated grafts compared to rapamycin-only ($n=4$ per group). Data are presented as means ± SD in **B**, **C**, **E**, **G**, **H**. Statistical analysis was performed using a 2-tailed unpaired Student's t-test; ns, $P>0.05$, $^{*}P<0.05$, $^{**}P<0.01$, and $^{***}P<0.001$. Scale bars: 100 μm in (**F**); 20 μm in (**D**)

follicle retention. The rapamycin group showed a higher number of retained follicles compared to the untreated group, while the VRCS group exhibited the greatest follicle retention (Fig. 5C, red arrows). Quantitative analysis revealed that the total number of remaining follicles in the untreated group was 74.5 ± 34.77 (1.75 ± 2.49 primordial, 27.75 ± 18.16 primary, 33.75 ± 13.55 secondary, and 11.25 ± 3.19 antral follicles) (Fig. 5D and E). In the rapamycin group, the number increased to 151.5 ± 29.06 (18.75 ± 9.68 primordial, 42.75 ± 9.63 primary, 67 ± 10.05 secondary, and 23 ± 8.15 antral follicles), while the VRCS group showed the highest follicle retention at 283 ± 71.93 (92.75 ± 58.46 primordial, 73 ± 12.02 primary, 91.25 ± 12.6 secondary, and 26 ± 4.95 antral follicles) (Fig. 5D and E). These results demonstrate that the protective effects of VRCS on the ovarian reserve persist up to four months post-transplantation, with outcomes superior to rapamycin treatment alone.

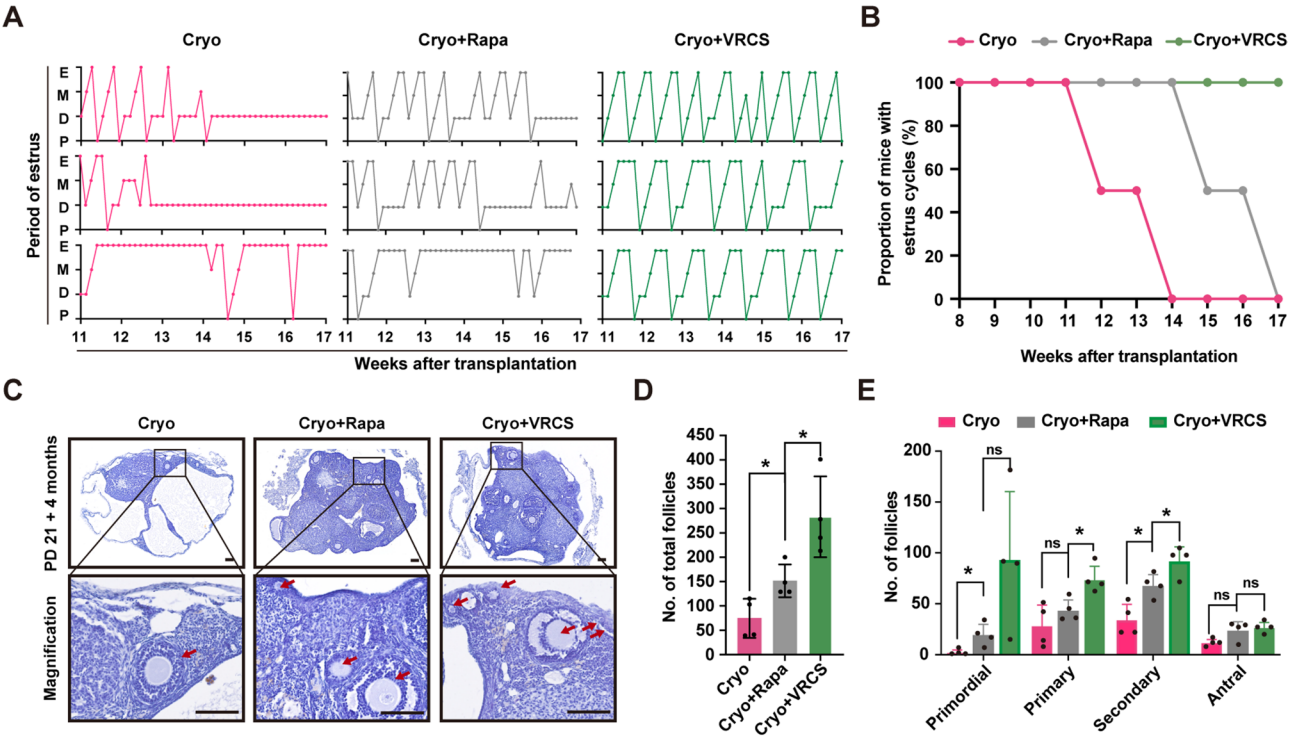

Fig. 5 VRCS prolongs female reproductive function after OTCT. **A**, Estrous cycles were monitored for 17 weeks in mice transplanted with untreated, rapamycin-treated, or VRCS-treated cryopreserved ovarian tissue, starting 8 weeks post-transplantation. **B**, Analysis of the estrous cycle revealed that 50% of the mice in the untreated group maintained regular cycles until week 11, with the remaining 50% showing regular cycles until week 13. In the rapamycin-treated group, 50% exhibited regular cycles until week 14, and the remaining mice until week 16. In contrast, all mice in the VRCS group maintained regular cycles throughout the entire monitoring period. **C**, Histology of ovarian grafts collected 4 months post-transplantation, showing remaining follicles (red arrows) in each treatment group (Hematoxylin staining). **D**, Quantification of the total number of remaining follicles in each group revealed a significant increase in the rapamycin group compared to the untreated group. The VRCS group showed the highest number of follicles, with a significant increase compared to both other groups ($n = 4$ for each group). **E**, Detailed quantification of follicle stages showed that the untreated group had the lowest numbers across most stages. The rapamycin group had higher counts and the VRCS group exhibited the greatest preservation of follicles across all stages, with significantly higher numbers than the other groups ($n = 4$ for each group). The data are presented as means ± SD in (**D**), (**E**). Statistical analysis was performed using a 2-tailed unpaired Student's t-test; ns, $P > 0.05$; $^*P < 0.05$. Scale bars: 100 μm

Discussion

OTCT has become an essential clinical approach for fertility preservation, leading to hundreds of successful live births [41]. However, a significant obstacle remains: the substantial loss of the ovarian reserve due to ischemia-reperfusion injury after transplantation [9, 10]. Transplanted grafts typically face a hypoxic environment for 3–5 days post-transplantation, relying solely on nutrient and oxygen diffusion from surrounding tissues [42]. This critical "window period" results in a considerable depletion of primordial follicles [43]. Our study mapped the ovarian reserve depletion curve in a mouse model, identifying the first three days post-transplantation as a phase of rapid follicle loss. Understanding this early phase is crucial for elucidating the mechanisms of follicle depletion in OTCT.

Our findings demonstrate that damage to tip cells, which are key players in angiogenesis [15, 44], is a primary driver of follicle loss after transplantation. Tip cells are essential for revascularization, and their reduction following cryopreservation and transplantation severely compromises the reconstruction of the vascular network. Using advanced imaging techniques with an endogenous fluorescent reporter mouse model [15], we showed that cryopreservation and thawing disrupt the intrinsic vascular architecture, leading to a decreased tip cell density and a reduced capacity for angiogenesis post-transplantation. These findings highlight the critical need for supporting vascular reconstruction to prevent ovarian reserve depletion.

In addition to vascular challenges, our study underscores the significant role of primordial follicle overactivation in depleting the ovarian reserve during OTCT. This overactivation is not solely a consequence of cryopreservation; it is also exacerbated by mechanical manipulation during early tissue handling. Our results suggest that administering rapamycin consistently throughout tissue isolation, cryopreservation, thawing, and pre-culture effectively suppresses follicle activation

continuously, potentially providing greater benefits than intermittent application of inhibitors.

While rapamycin effectively reduces follicle overactivation, it may also impact ovulation and oocyte developmental potential negatively. In our study, ovaries treated solely with rapamycin produced fewer oocytes during superovulation and displayed reduced rates of two-cell embryo and blastocyst formation. This effect may be related to rapamycin's inhibition of the PI3K pathway in developing follicles [45], which remain active by day 14 post-transplantation. Moreover, studies have shown that rapamycin inhibits angiogenesis by downregulating VEGFA expression and its downstream VEGFR signaling pathway [46, 47]. This inhibition may further aggravate ischemia-reperfusion injury after tissue transplantation, elevate reactive oxygen species (ROS) production, and compromise oocyte quality [48]. Interestingly, the addition of VEGFA appears to counterbalance these adverse effects by enhancing both ovulation and fertilization outcomes. However, the precise mechanisms by which VEGFA improves oocyte quality remain to be fully elucidated and warrant further investigation.

Although our study presents a promising strategy for preserving ovarian reserve in OTCT, several limitations may affect the translation of these findings to clinical practice. First, while bisected mouse ovaries provide a convenient and reproducible model for studying transplantation and injury, they do not fully replicate the structure or clinical handling of human ovarian cortical tissue. Second, although vitrification offers advantages such as speed and reduced ice crystal formation, it differs from the computer-controlled slow freezing method commonly used in previous studies [5]. Despite these limitations, the VRCS approach still holds potential for preserving fertility and endocrine function in women undergoing gonadotoxic treatments, such as chemotherapy, thereby supporting long-term quality of life.

Conclusions

The VEGFA-Rapamycin Combination Strategy (VRCS) demonstrates distinct advantages over using rapamycin or VEGFA alone. By promoting angiogenesis, enhancing vascular reconstruction, and consistently suppressing primordial follicle activation, VRCS offers more effective protection of the ovarian reserve following transplantation. To translate this approach into clinical practice, future studies using human samples are needed for validation. If successful, VRCS could significantly improve OTCT outcomes and provide renewed hope for fertility preservation in patients undergoing gonadotoxic treatments enhancing the ovarian reserve preservation and endocrine function restoration effect of patients.

Abbreviations

OTCT	Ovarian Tissue Cryopreservation and Transplantation
VEGFA	Vascular Endothelial Growth Factor A
mTORC1	mammalian Target Of Rapamycin Complex 1
PI3K	Phosphatidylinositol 3 Kinase
MII	Metaphase II
DDX4	DEAD-box helicase 4
DEPs	Differentially Expressed Proteins
KEGG	Kyoto Encyclopedia of Genes and Genomes
GO	Gene Ontology
HIF-1	Hypoxia-Inducible factor 1
Akt	Protein Kinase B
FoxO	Forkhead box O
GFP	Green Fluorescent Protein
Cryo	Cryopreservation
Rapa	Rapamycin
VRCS	VEGFA-Rapamycin Combination Strategy
SPF	Specific Pathogen-Free
DMSO	Dimethyl Sulfoxide
EG	Ethylene Glycol
PFA	Paraformaldehyde
BSA	Bovine Serum Albumin
PMSG	Pregnant Mare Serum Gonadotropin
hCG	Human Chorionic Gonadotropin
COCs	Cumulus-Oocyte Complexes

Supplementary Information

The online version contains supplementary material available at https://doi.org/10.1186/s12958-025-01422-y.

Supplementary Material 1: Figure S1 Follicle over-activation and inadequate angiogenesis contribute to rapid follicle loss in cryopreserved ovaries. A, Schematic of the proteomic analysis: Ovaries from PD21 mice were isolated, cryopreserved, and recovered as described in Fig. 1A. B, Gene Ontology (GO) enrichment analysis of differentially expressed proteins (DEPs), GO terms related to blood vessel development and maintained was shown in blue text. GO terms with corrected P-values < 0.05 were considered significantly enriched.

Supplementary Material 2: Table S1: differentially expressed proteins in cryopreserved vs. fresh ovarian samples: mass spectrometry analysis. The "All list" table presents a comprehensive list of all proteins detected after removing duplicates, errors, and redundant data from the protein mass spectrometry database search results. In this table, column E, F indicates the protein expression levels detected in fresh ovarian samples by mass spectrometry, while column G displays the average of the two columns. Column H, I represents the protein expression levels detected in cryopreserved ovarian samples, and column J shows the average of the two columns. The "Down regulation list," "Up regulation list," and "No significance list" sheets show the results of the comparison between the cryopreserved and fresh groups. A Student's t-test was used to assess the significance of differences. $P < 0.05$ indicates statistical significance. Fold change < 0.67 denotes downregulation of protein expression, Fold change > 1.5 indicates upregulation of protein expression.

Acknowledgements

Sincerely gratitude to the Mass Spectrometry Platform at China Agricultural University for providing technical support in protein mass spectrometry experiments, data quality assessment, and data analysis for this research.

Author contributions

L.L., J.Y., J.Z., Y.Z. and H.Z. designed the research; L.L., J.Y., L.J., J.L., K.C., X.Y., L.M., G.W., K.G., and Q.H. performed the experiments; L.L., J.Y., L.J., Y.Z. and H.Z. analyzed the data; X.X., G.X., J.Z., Y.Z. and H.Z. supervised the research work; L.L., J.Y., draw the graphic model; L.L., J.Y., J.Z., Y.Z. and H.Z. wrote the paper; L.L., J.Y., K.C., X.Y., T.G., Y.Z., J.Z. and H.Z. revised and proofread the manuscript; Z.L. provided proteomics-related experiments and data analysis methods; All authors have seen and approved the final version.

Funding
This work was supported by the National Key Research and Development Program of China to H.Z. (2022YFC2703800, 2024YFC2706600), the Key Program of National Natural Science Foundation of China to H.Z. (82230051), the Innovative Project of State Key Laboratory of Animal Biotech Breeding to H.Z. (2023SKLAB1-6), the Chinese Universities Scientific Fund to H.Z. (2024TC017), the National Natural Science Foundation of China to Y.Z. (82371664), the 2115 Talent Development Program of China Agricultural University to Y.Z. and the National Natural Science Foundation of China to J.Z. (32200704), and the National Key Research & Developmental Program of China (2022YFC2703000) to T.G.

Data availability
The mass spectrometric raw data were submitted in ProteomeXchange, and the PXD number is PXD061025 (https://www.iprox.cn/page/project.html?id=IPX0011049000).

Declarations

Ethics approval and consent to participate
All animal experiments were approved by the Committee on the Ethics of Animal Experiments at China Agricultural University, NO. AW11104202-3-1.

Consent for publication
Not applicable.

Competing interests
The authors declare no competing interests.

Author details
[1]State Key Laboratory of Animal Biotech Breeding, College of Biological Sciences, China Agricultural University, Beijing 100193, China
[2]Institute of Women, Children, and Reproductive Health, Shandong University, Ji'nan, Shandong 250012, China
[3]IDG/McGovern Institute for Brain Research, School of Life Sciences, Tsinghua University, Beijing 100084, China
[4]Biomedical Pioneering Innovation Center, School of Life Sciences, Peking University, Beijing 100871, China
[5]Peking-Tsinghua Center for Life Sciences, Academy for Advanced Interdisciplinary Studies, Peking University, Beijing 100871, China
[6]College of Animal Science and Technology, Northeast Agricultural University, Harbin 150030, China

Received: 24 March 2025 / Accepted: 21 May 2025
Published online: 03 July 2025

References

1. Spears N, Lopes F, Stefansdottir A, Rossi V, De Felici M, Anderson RA, et al. Ovarian damage from chemotherapy and current approaches to its protection. Hum Reprod Update. 2019;25(6):673–93.
2. Wallace WH, Smith AG, Kelsey TW, Edgar AE, Anderson RA. Fertility preservation for girls and young women with cancer: population-based validation of criteria for ovarian tissue cryopreservation. Lancet Oncol. 2014;15(10):1129–36.
3. Donnez J, Dolmans MM. Fertility preservation in women. N Engl J Med. 2018;378(4):400–1.
4. Khattak H, Malhas R, Craciunas L, Afifi Y, Amorim CA, Fishel S, et al. Fresh and cryopreserved ovarian tissue transplantation for preserving reproductive and endocrine function: a systematic review and individual patient data meta-analysis. Hum Reprod Update. 2022;28(3):400–16.
5. Ramirez T, Pavone M. Exploring the frontiers of ovarian tissue cryopreservation: a review. J Clin Med. 2024;13(15):4513.
6. Shapira M, Dolmans MM, Silber S, Meirow D. Evaluation of ovarian tissue transplantation: results from three clinical centers. Fertil Steril. 2020;114(2):388–97.
7. Donnez J, Dolmans MM. Ovarian cortex transplantation: 60 reported live births brings the success and worldwide expansion of the technique towards routine clinical practice. J Assist Reprod Genet. 2015;32(8):1167–70.
8. Lotz L, Dittrich R, Hoffmann I, Beckmann MW. Ovarian tissue transplantation: experience from Germany and worldwide efficacy. Clin Med Insights Reprod Health. 2019;13:1179558119867357.
9. Gavish Z, Spector I, Peer G, Schlatt S, Wistuba J, Roness H, et al. Follicle activation is a significant and immediate cause of follicle loss after ovarian tissue transplantation. J Assist Reprod Gen. 2018;35(1):61–9.
10. Cacciottola L, Manavella DD, Amorim CA, Donnez J, Dolmans MM. In vivo characterization of metabolic activity and oxidative stress in grafted human ovarian tissue using Microdialysis. Fertil Steril. 2018;110(3):534–44. e3.
11. Manavella DD, Cacciottola L, Pomme S, Desmet CM, Jordan BF, Donnez J, et al. Two-step transplantation with adipose tissue-derived stem cells increases follicle survival by enhancing vascularization in xenografted frozen-thawed human ovarian tissue. Hum Reprod. 2018;33(6):1107–16.
12. Israely T, Nevo N, Harmelin A, Neeman M, Tsafiri A. Reducing ischaemic damage in rodent ovarian xenografts transplanted into granulation tissue. Hum Reprod. 2006;21(6):1368–79.
13. Manavella DD, Cacciottola L, Payen VL, Amorim CA, Donnez J, Dolmans MM. Adipose tissue-derived stem cells boost vascularization in grafted ovarian tissue by growth factor secretion and differentiation into endothelial cell lineages. Mol Hum Reprod. 2019;25(4):184–93.
14. Macchiarelli G, Jiang JY, Nottola SA, Sato E. Morphological patterns of angiogenesis in ovarian follicle capillary networks. A scanning electron microscopy study of corrosion cast. Microsc Res Tech. 2006;69(6):459–68.
15. Xu X, Mu L, Li L, Liang J, Zhang S, Jia L, et al. Imaging and tracing the pattern of adult ovarian angiogenesis implies a strategy against female reproductive aging. Sci Adv. 2022;8(2):eabi8683.
16. Otani N, Minami S, Yamoto M, Shikone T, Otani H, Nishiyama R, et al. The vascular endothelial growth factor/fms-like tyrosine kinase system in human ovary during the menstrual cycle and early pregnancy. J Clin Endocrinol Metab. 1999;84(10):3845–51.
17. Dissen GA, Lara HE, Fahrenbach WH, Costa ME, Ojeda SR. Immature rat ovaries become revascularized rapidly after autotransplantation and show a gonadotropin-dependent increase in angiogenic factor gene-expression. Endocrinology. 1994;134(3):1146–54.
18. Kang BJ, Wang Y, Zhang L, Xiao Z, Li SW. bFGF and VEGF improve the quality of vitrified-thawed human ovarian tissues after xenotransplantation to SCID mice. J Assist Reprod Genet. 2016;33(2):281–9.
19. Cacciottola L, Nguyen TYT, Amorim CA, Donnez J, Dolmans MM. Modulating hypoxia and oxidative stress in human xenografts using adipose tissue-derived stem cells. F S Sci. 2021;2(2):141–52.
20. Manavella DD, Cacciottola L, Pommé S, Desmet CM, Jordan BF, Donnez J, et al. Two-step transplantation with adipose tissue-derived stem cells increases follicle survival by enhancing vascularization in xenografted frozen-thawed human ovarian tissue. Hum Reprod. 2018;33(6):1107–16.
21. Terren C, Munaut C. Molecular basis associated with the control of primordial follicle activation during transplantation of cryopreserved ovarian tissue. Reprod Sci. 2021;28(5):1257–66.
22. Zhang H, Liu K. Cellular and molecular regulation of the activation of mammalian primordial follicles: somatic cells initiate follicle activation in adulthood. Hum Reprod Update. 2015;21(6):779–86.
23. Reddy P, Zheng W, Liu K. Mechanisms maintaining the dormancy and survival of mammalian primordial follicles. Trends Endocrinol Metab. 2010;21(2):96–103.
24. Liu W, Zhang J, Wang L, Liang S, Xu B, Ying X, et al. The protective effects of Rapamycin pretreatment on ovarian damage during ovarian tissue cryopreservation and transplantation. Biochem Biophys Res Commun. 2021;534:780–6.
25. Bindels J, Squatrito M, Bernet L, Nisolle M, Henry L, Munaut C. The mTOR inhibitor Rapamycin counteracts follicle activation induced by ovarian cryopreservation in murine transplantation models. Med (Kaunas). 2023;59(8):1474.
26. Grosbois J, Demeestere I. Dynamics of PI3K and Hippo signaling pathways during in vitro human follicle activation. Hum Reprod. 2018;33(9):1705–14.
27. Zheng WJ, Zhang H, Gorre N, Risal S, Shen Y, Liu K. Two classes of ovarian primordial follicles exhibit distinct developmental dynamics and physiological functions. Hum Mol Genet. 2014;23(4):920–8.
28. Cao J, Jin L, Yan ZQ, Wang XK, Li YY, Wang Z, et al. Reassessing endothelial-to-mesenchymal transition in mouse bone marrow: insights from lineage tracing models. Nat Commun. 2023;14(1):8461.
29. Zhang J, Yan L, Wang Y, Zhang S, Xu X, Dai Y, et al. In vivo and in vitro activation of dormant primordial follicles by EGF treatment in mouse and human. Clin Transl Med. 2020;10(5):e182.

30. Langbeen A, Ginneken CV, Fransen E, Bosmans E, Leroy J, Bols PEJ. Morphometrical analysis of preantral follicular survival of VEGF-treated bovine ovarian cortex tissue following xenotransplantation in an immune deficient mouse model. Anim Reprod Sci. 2016;168:73–85.
31. Cunha GR, Baskin L. Use of sub-renal capsule transplantation in developmental biology. Differentiation. 2016;91(4–5):4–9.
32. Cora MC, Kooistra L, Travlos G. Vaginal cytology of the laboratory rat and mouse: review and criteria for the staging of the estrous cycle using stained vaginal smears. Toxicol Pathol. 2015;43(6):776–93.
33. Zhang Y, Wang Y, Feng X, Zhang S, Xu X, Li L, et al. Oocyte-derived microvilli control female fertility by optimizing ovarian follicle selection in mice. Nat Commun. 2021;12(1):2523.
34. Greaney J, Subramanian GN, Ye Y, Homer H. Isolation and in vitro culture of mouse oocytes. Bio Protoc. 2021;11(15):e4104.
35. Wisniewski JR, Zougman A, Nagaraj N, Mann M. Universal sample Preparation method for proteome analysis. Nat Methods. 2009;6(5):359–62.
36. Zhou Y, Zhou B, Pache L, Chang M, Khodabakhshi AH, Tanaseichuk O, et al. Metascape provides a biologist-oriented resource for the analysis of systems-level datasets. Nat Commun. 2019;10(1):1523.
37. Faire M, Skillern A, Arora R, Nguyen DH, Wang J, Chamberlain C, et al. Follicle dynamics and global organization in the intact mouse ovary. Dev Biol. 2015;403(1):69–79.
38. John GB, Gallardo TD, Shirley LJ, Castrillon DH. Foxo3 is a PI3K-dependent molecular switch controlling the initiation of oocyte growth. Dev Biol. 2008;321(1):197–204.
39. Dai Y, Bo Y, Wang P, Xu X, Singh M, Jia L, et al. Asynchronous embryonic germ cell development leads to a heterogeneity of postnatal ovarian follicle activation and May influence the timing of puberty onset in mice. BMC Biol. 2022;20(1):109.
40. Zhang H, Risal S, Gorre N, Busayavalasa K, Li X, Shen Y, et al. Somatic cells initiate primordial follicle activation and govern the development of dormant oocytes in mice. Curr Biol. 2014;24(21):2501–8.
41. Dolmans MM, Falcone T, Patrizio P. Importance of patient selection to analyze in vitro fertilization outcome with transplanted cryopreserved ovarian tissue. Fertil Steril. 2020;114(2):279–80.
42. Rahimi G, Isachenko V, Kreienberg R, Sauer H, Todorov P, Tawadros S, et al. Re-vascularisation in human ovarian tissue after conventional freezing or vitrification and xenotransplantation. Eur J Obstet Gyn R B. 2010;149(1):63–7.
43. Nisolle M, Casanas-Roux F, Qu J, Motta P, Donnez J. Histologic and ultrastructural evaluation of fresh and frozen-thawed human ovarian xenografts in nude mice. Fertil Steril. 2000;74(1):122–9.
44. Pan X, Li X, Dong L, Liu T, Zhang M, Zhang LN, et al. Tumour vasculature at single-cell resolution. Nature. 2024;632(8024):429–36.
45. Dou X, Sun Y, Li J, Zhang J, Hao D, Liu W, et al. Short-term Rapamycin treatment increases ovarian lifespan in young and middle-aged female mice. Aging Cell. 2017;16(4):825–36.
46. Wang M, Xu Y, Wen GZ, Wang Q, Yuan SM. Rapamycin suppresses angiogenesis and lymphangiogenesis in melanoma by downregulating VEGF-A/VEGFR-2 and VEGF-C/VEGFR-3 expression. Onco Targets Ther. 2019;12:4643–54.
47. Liu XM, Zhu WT, Jia ML, Li YT, Hong Y, Liu ZQ, et al. Rapamycin liposomes combined with 5-Fluorouracil inhibits angiogenesis and tumor growth of APC ((Min/+)) mice and AOM/DSS-Induced colorectal Cancer mice. Int J Nanomed. 2022;17:5049–61.
48. Li X, Chen C, Dai Y, Huang C, Han Q, Jing L, et al. Cinobufagin suppresses colorectal cancer angiogenesis by disrupting the endothelial mammalian target of rapamycin/hypoxia-inducible factor 1alpha axis. Cancer Sci. 2019;110(5):1724–34.

Publisher's note